Original Article

MOLECULAR METABOLISM

Specific knockout of p85α in brown adipose tissue induces resistance to high-fat diet–induced obesity and its metabolic complications in male mice

Almudena Gomez-Hernandez [1,2,3,*], Andrea R. Lopez-Pastor [1,2,5], Carlota Rubio-Longas [1,5], Patrik Majewski [1,5], Nuria Beneit [1,2], Vanesa Viana-Huete [1,2], Gema García-Gómez [2,3], Silvia Fernandez [2,3], Marta Letizia Hribal [4], Giorgio Sesti [4], Oscar Escribano [1,2,3], Manuel Benito [1,2,3]

ABSTRACT

Objective: An increase in mass and/or brown adipose tissue (BAT) functionality leads to an increase in energy expenditure, which may be beneficial for the prevention and treatment of obesity. Moreover, distinct class I PI3K isoforms can participate in metabolic control as well as in systemic dysfunctions associated with obesity. In this regard, we analyzed *in vivo* whether the lack of p85α in BAT (BATp85αKO) could modulate the activity and insulin signaling of this tissue, thereby improving diet-induced obesity and its associated metabolic complications.
Methods: We generated BATp85αKO mice using Cre-LoxP technology, specifically deleting p85α in a conditional manner. To characterize this new mouse model, we used mice of 6 and 12 months of age. In addition, BATp85αKO mice were submitted to a high-fat diet (HFD) to challenge BAT functionality.
Results: Our results suggest that the loss of p85α in BAT improves its thermogenic functionality, high-fat diet–induced adiposity and body weight, insulin resistance, and liver steatosis. The potential mechanisms involved in the improvement of obesity include (1) increased insulin signaling and lower activation of JNK in BAT, (2) enhanced insulin receptor isoform B (IRB) expression and association with IRS-1 in BAT, (3) lower production of proinflammatory cytokines by the adipose organ, (4) increased iWAT browning, and (5) improved liver steatosis.
Conclusions: Our results provide new mechanisms involved in the resistance to obesity development, supporting the hypothesis that the gain of BAT activity induced by the lack of p85α has a direct impact on the prevention of diet-induced obesity and its associated metabolic complications.

Keywords Obesity; Insulin resistance; Brown adipose tissue; White adipose tissue; p85α

1. INTRODUCTION

Obesity can be defined as a chronic disease of multifactorial origin in which the imbalance between food intake and energy expenditure leads to an abnormal increase in body fat storage. The incidence of obesity has increased over the past decades in developed countries, and it is currently considered a global epidemic [1]. In 2014, 39% of adults were overweight, and 13% of them suffered from obesity. Obesity is also a huge public health problem because of the risk of other associated pathologies, such as diabetes, ischemic heart disease, and a higher incidence of gastrointestinal cancers in obese individuals [1]. Increased adiposity induces the expression of proinflammatory cytokines, triggering early primary insulin resistance,

[1]Biochemistry and Molecular Biology Department, School of Pharmacy, Complutense University of Madrid, Spain [2]Health Research Institute of San Carlos Clinic Hospital (IdISSC), Madrid, Spain [3]CIBER of Diabetes and Associated Metabolic Diseases (CIBERDEM), Spain [4]Department of Medical and Surgical Sciences, University Magna Graecia of Catanzaro, Italy

[5] These authors contributed equally.

*Corresponding author. Biochemistry and Molecular Biology Department, School of Pharmacy, Complutense University of Madrid, Plaza. Ramón y Cajal s/n, Madrid, 28040, Spain. Fax: +34 91 3941779.

E-mails: algomezh@ucm.es, algomezh@ucm.es (A. Gomez-Hernandez), andreara@ucm.es (A.R. Lopez-Pastor), carrub05@ucm.es (C. Rubio-Longas), patmajewski94@gmail.com (P. Majewski), nubere87@hotmail.com (N. Beneit), vanesa.viana.h@gmail.com (V. Viana-Huete), ggarciag@ucm.es (G. García-Gómez), silferna@ucm.es (S. Fernandez), hribal@unicz.it (M.L. Hribal), sesti@unicz.it (G. Sesti), oescriba@ucm.es (O. Escribano), mbenito@ucm.es (M. Benito).

Abbreviations: BATp85αKO, Brown adipose tissue–specific p85alpha knockout; gWAT, gonadal white adipose tissue; IR, insulin receptor; iWAT, inguinal white adipose tissue; PI3K, phosphatidylinositol 3-kinase; qRT-PCR, real-time quantitative polymerase chain reaction; rtWAT, retroperitoneal white adipose tissue; vWAT, visceral white adipose tissue

Received August 5, 2019 • Revision received October 14, 2019 • Accepted October 30, 2019 • Available online 9 November 2019

https://doi.org/10.1016/j.molmet.2019.10.010

lipid mobilization to peripheral tissues, and the development of systemic insulin resistance [2].

In mammals, the adipose organ is composed of two types of adipose tissue: white adipose tissue (WAT) and brown adipose tissue (BAT), which have different morphology, distribution, gene expression and function. The development of obesity depends not only on the balance between intake and energy consumption but also on the balance between these two kinds of adipose tissue [3]. Currently, both these types of adipose tissue are widely considered as endocrine organs. The main adipokines secreted by WAT, such as leptin and adiponectin, are also expressed in BAT, especially when its thermogenic function is activated [4]. However, BAT can secrete other autocrine or paracrine factors.

In 2009, it was described for the first time that in humans, the amount of functional BAT is inversely related to body mass index, especially in elderly people [5]. Thus, in recent years, the thermogenic capacity of BAT in humans has been highlighted as a possible target for the prevention and treatment of obesity because of its capacity to increase energy expenditure, which has a direct effect on carbohydrate and lipid metabolism [6,7].

On the other hand, PI3Ks are members of a conserved family of enzymes responsible for the phosphorylation of proteins and lipids. PI3K isoforms have been categorized into three classes (class I, II, and III) according to their lipid substrate preferences and their structural features [8,9]. Class I PI3Ks are formed by heterodimers of a catalytic subunit and a regulatory subunit. Three different genes give rise to different regulatory subunits: PIK3R1, which encodes p85α and its splice isoforms p55α and p50α; PIK3R2, which encodes p85β; and PIK3R3, which encodes p55γ. The catalytic subunits also arise from three genes: PIK3CA, PIK3CB, and PIK3CD, encoding p110α, p110β, and p110δ, respectively [10,11]. Depending on the activation mechanism and the differential association with regulatory subunits, class I PI3Ks have been grouped in two subfamilies, class IA and class IB. Class IA catalytic subunits bind to the p85 type of regulatory subunits, which are able to bind to phosphorylated tyrosines on receptor tyrosine kinases and adaptors, such as IR substrates (IRSs) [12]. Moreover, distinct class I PI3K isoforms can participate at different levels in metabolic control as well as in systemic dysfunctions associated with obesity. Functional insulin signaling is essential in patients with obesity, allowing the storage of lipids in an efficient manner within the adipose depots [13].

Taking into account that the lack of p85α [14–16] induces an increased insulin sensitivity in mice, we hypothesized that a new mouse model lacking p85α in BAT (BATp85αKO) would increase insulin signaling and brown fat functionality, conferring resistance to diet-induced obesity and its associated metabolic complications. Thus, we have primarily generated BATp85αKO mice in a tissue-specific manner using Cre-LoxP technology to induce the lack of p85α exclusively in this tissue. To characterize this new mouse model, we studied control and BATp85αKO mice at 6 and 12 months of age. Moreover, other groups of mice, fed a high-fat diet (HFD), were used to study their response to an obesity challenge.

2. MATERIALS AND METHODS

2.1. Experimental models

Male mice were maintained on a 12-hour light–dark cycle at 23 °C (room temperature). All animals used had a C57BL/6 genetic background. In this study, we generated for the first time a model specifically lacking p85α in BAT (BATp85αKO) using Cre-LoxP technology. Cre recombinase expression was controlled by the UCP-1 promoter, inducing p85α ablation in BAT. Two loxP sites were inserted to flank exon 7 as previously described [17]. The control group included p85$\alpha^{loxP/loxP}$ and wild-type (WT) C57BL/6 mice. Transgenic mice expressing the Cre recombinase have been previously described [18]. In a first set of experiments, we used control and BATp85αKO mice at 6 and 12 months of age fed a standard diet (STD) to characterize the new model. For that, we used 27 mice: control 6 m (n = 4), BATp85αKO 6 m (n = 7), control 12 m (n = 10), and BATp85αKO 12 m (n = 6). In a second set of experiments, other groups of control and BATp85αKO mice were submitted to an HFD to assess their thermogenic capacity and whether they could show resistance to obesity development in these conditions. Thus, 6-week-old male control and BATp85αKO mice were fed an STD (3% kcal from fat) or an HFD (Ref. TD06414, 60.3% kcal from fat) for 10 weeks and were sacrificed at 16 weeks of age. In this approach, we used 25 mice, divided into four groups: control STD (n = 5), BATp85αKO STD (n = 5), control HFD (n = 8), and BATp85αKO HFD (n = 7). Anesthetized mice (Avertin, 250 mg/kg, intraperitoneally) were saline perfused.

The liver was embedded in Tissue-Tek® optimum cutting temperature compound and frozen for histological analysis; other tissues, including other sections from the liver, were maintained in formalin to be included in paraffin for histological studies or alternatively were frozen for protein and RNA isolation. All animal experimentation procedures described in this manuscript were conducted according to accepted standards of human animal care, as approved by the institutional committee of Complutense University of Madrid. All animal procedures were performed according to the guidelines from Directive 2010/63/EU of the European Parliament and the National Institutes of Health on the protection of animals used for scientific purposes.

p85α loxP/loxP and UCP-1-Cre transgenic mice were genotyped by polymerase chain reaction (PCR). Tail DNA (100–200 ng) was amplified in 30 cycles (40 s, 94 °C; 40 s, 60 °C; and 1 min, 75 °C) by a thermal cycler. Two primers flanking the loxP site behind exon 7 of the p85α were used: M85AG6>7A: GGTTTCTTACTTTAGACGGAGCTG and M85AG7>6B: CATAATTTCATGTGCCATGGAAGAC. A 460-bp band was obtained for the floxed allele or, a 270-bp band was used for the WT allele. UCP-1-Cre transgenic mice were genotyped as previously described [19]. In addition, the Cre-mediated deletion of exon 7 of the *Pik3r1* gene in BAT was also verified by PCR using the primer pair ACGGAATGGAATGAGAGACAGC and AAGAGTGTAATCGCCGTGCAT, which amplifies a 225-bp fragment from the undeleted allele and an 103-bp fragment from the deleted allele.

2.2. Analytical procedures

Plasma levels of insulin were analyzed using enzyme-linked immunosorbent assay (ELISA) kits (Millipore). Cholesterol and triglycerides were tested in plasma samples from fasted mice (Spinreact). Blood glucose level was determined in fasted animals using an automatic monitor (Roche Molecular Biochemicals GmbH). Glucose and insulin tolerance tests were performed as previously described [19].

2.3. Thermogenic response to cold exposure

For the acute cold exposure experiments, we used 16-week-old control and BATp85αKO mice under an HFD as well as 12-month-old control and BATp85αKO mice. Animals were acclimatized to thermoneutrality (28 °C) for 3 days and then transferred to 4 °C for 12 h with full access to water and food. Body temperature was periodically measured by using a digital thermometer with a colonic probe (BIO-9882; Bioseb).

2.4. *In vivo* insulin signaling studies

Mice were injected with 1 U/kg body weight of human insulin (Novo Nordisk) into the peritoneal cavity. After 10 min, mice were euthanized with 250 mg/kg Avertin. Tissues were then removed and immediately frozen in liquid nitrogen. We performed western blotting to analyze phospho-protein kinase B (Akt) (T308) in BAT, gWAT (gonadal depot), and iWAT (inguinal depot).

2.5. Histological analysis

Paraffin-embedded BAT, gWAT, and iWAT were cross-sectioned into 4-μm-thick specimen at 5-mm intervals, dewaxed, and rehydrated. Paraffin-embedded sections were stained with hematoxylin and eosin to measure the adipocyte size (ImageJ Software).

Livers were optimal cutting temperature embedded, and sections of 7 μm were stained with Oil Red O/hematoxylin to measure lipid depots. p85α and UCP-1 were detected by immunoperoxidase with rabbit anti-p85α polyclonal antibody (ABS234) and rabbit anti-UCP-1 polyclonal antibody (ab10983), respectively. After an overnight incubation with each primary antibody, we incubated with a peroxidase-conjugated secondary antibody for 1 h at 1:200 dilutions. The sections were stained for 10 min at room temperature with 3,3-diaminobenzidine and then counterstained with hematoxylin and mounted in Ibidi mounting medium (Ibidi GmbH). In each experiment, negative controls without the primary antibody or using a nonrelated antibody were included to check for nonspecific staining.

The immunohistochemistry images were quantified using the "count and measure objects" tool in the Image-Pro Plus software. The color considered as positive staining for the same protein was manually selected, and the value corresponding to the sum of all stained areas was obtained. The results were expressed as the percentage of the stained area with respect to the total area analyzed in each sample.

2.6. Nuclear magnetic resonance imaging (NMRI)

Sixteen-week-old control HFD and BATp85αKO HFD male mice were anesthetized, and electrocardiogram and respiration were continuously monitored. Fat was measured by NMRI. The coil was positioned over

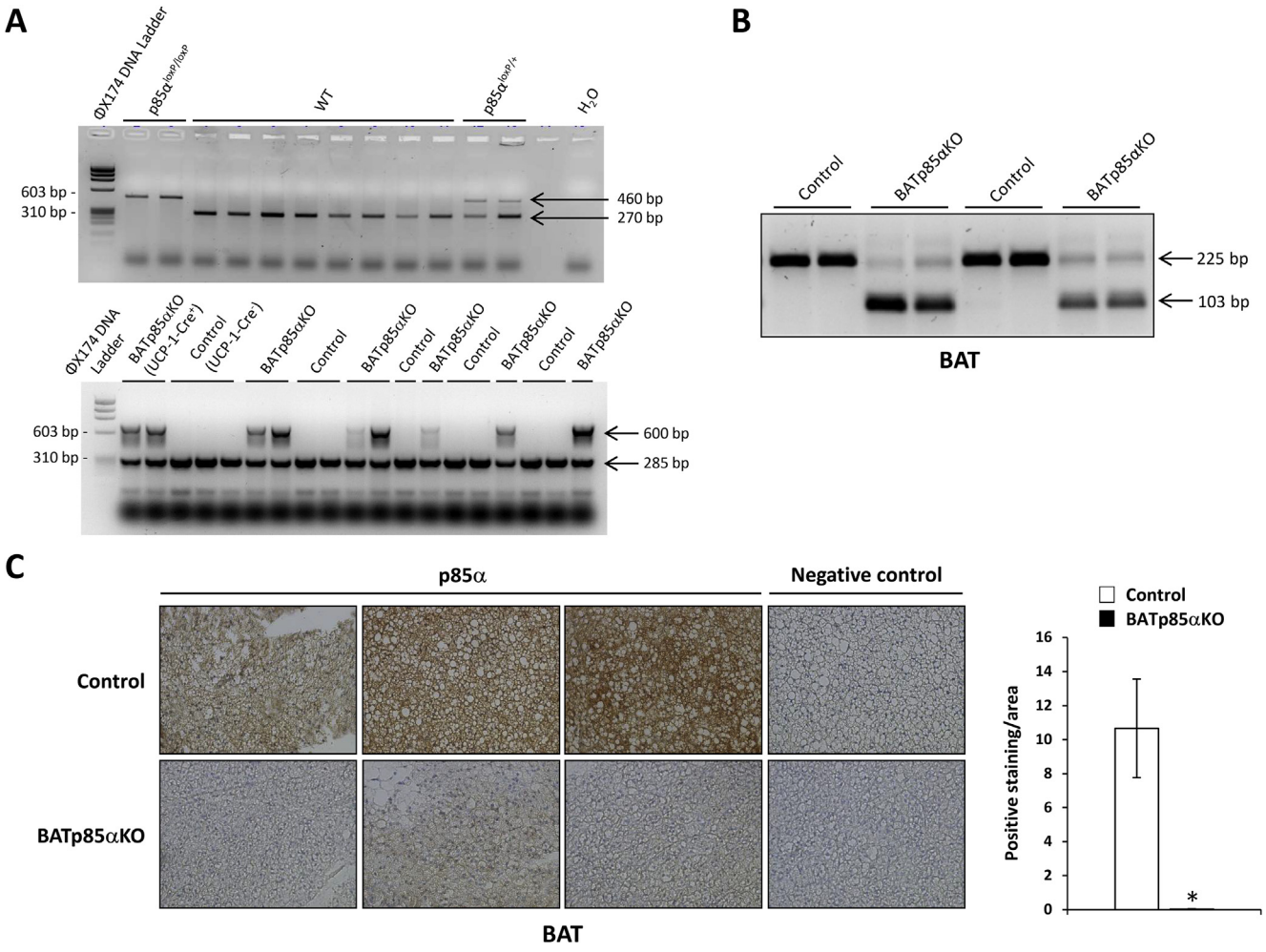

Figure 1: Characterization of BATp85αKO mice. (A) Representative gels of PCR for p85α$^{loxP/loxP}$ (upper panel) and UCP-1 Cre recombinase. In the upper gel, a 460-bp band was obtained for the floxed allele and a 270-bp band for the WT allele. As positive control, p85α$^{loxP/+}$ mice were used to obtain two bands. In the lower gel, a 600-bp band and a 285-bp band were obtained for BATp85αKO mice and only a 285-bp band for control mice. **(B)** The Cre-mediated deletion of exon 7 of the *p85α* gene was verified by PCR. We observed a 225-bp fragment from the undeleted p85 loxP allele and a 103-bp fragment from the deleted allele. **(C)** Representative microphotographs of immunohistochemistry against p85α and its quantification to assess the presence or absence of this regulatory subunit in BAT from BATp85αKO or control mice, respectively. Image magnification: 20 ×. Negative controls without the primary antibody were included to check for nonspecific staining. Results are expressed as mean ± SEM. Statistical significance was assessed by two-tailed unpaired *t*-test by comparison with control mice (*$p < 0.05$).

the epididymal fat in the abdomen. NMRI measurements were performed using a Bruker BIOSPEC 47/40 spectrometer (Bruker GmbH) operating at 4.7 T (200 MHz) superconducting magnet (Oxford Instruments Ltd) and high-performance actively shielded gradients with a maximum gradient strength of 50 mT/m. Data were collected as 256 × 128 matrices using the standard Bruker RARE_MOD (fast spin-echo) sequence, which yields T2-weighted images. The results were represented as fat body volume versus total body volume using ImageJ Launcher 1.46 software.

2.7. Western blot

Western blot analyses were performed on protein extracts from murine samples of BAT and WAT as previously described [20]. The antibodies used were IRβ and IGF-IRβ from Santa Cruz Biotechnology (Dallas, TX, USA); IRS-1 from Millipore (Billerica, MA, USA); UCP-1 from Abcam; p-Akt (Thr308), p-JNK (T183/Y185), p-AMPK (T172), and AMPK from Cell Signaling Technology (Danvers, MA, USA); and β-actin and α-tubulin from Sigma–Aldrich Corp. (St. Louis, MO, USA).

2.8. Immunoprecipitations

A total of 150 μg protein from BAT from control and BATp85αKO mice under HFD was immunoprecipitated at 4 °C with anti–insulin receptor isoform B (IRB) isoform antibody (provided by Dr Sesti and Dr Hribal). Supernatants were subsequently immunoprecipitated with anti-IRβ antibody recognizing both IR isoforms. Thus, immune complexes from the first (only IRB isoform) or the second (only IRA isoform) immunoprecipitations were collected on protein A–agarose beads and submitted to sodium dodecyl sulfate–polyacrylamide gel electrophoresis. Finally, immunoblots were incubated with anti-IRB or anti-IRβ antibodies to analyze the expression of IRB and IRA, respectively. To study the association between IR isoforms and IRS-1, immunoblots were reincubated with anti-IRS-1 antibody.

2.9. RNA extraction and real-time quantitative PCR

Total RNA was isolated from BAT and WAT by using TRIzol reagent (Invitrogen, Carlsbad, CA) and quantified by absorbance at 260 nm. One microgram of RNA was used to perform the reverse transcription with a high-capacity cDNA archive kit (Applied Biosystems, Foster City, CA). Real-time quantitative PCR (qRT-PCR) was performed on an ABI Prism 7900 PCR system (Applied Biosystems) according to the manufacturer's protocol, using the ΔΔCt method as previously described [20]. Thus, the amount of target, normalized to endogenous gene and relative to the control, is given by relative quantification (RQ) $= 2^{-\Delta\Delta Ct}$; ΔCt (cycle threshold) = Ct (target gene) − Ct (*Gapdh*); ΔΔCt = ΔCt for any sample − ΔCt for the control. Amplification of *Gapdh* was used in the same reaction of all samples as an internal control.

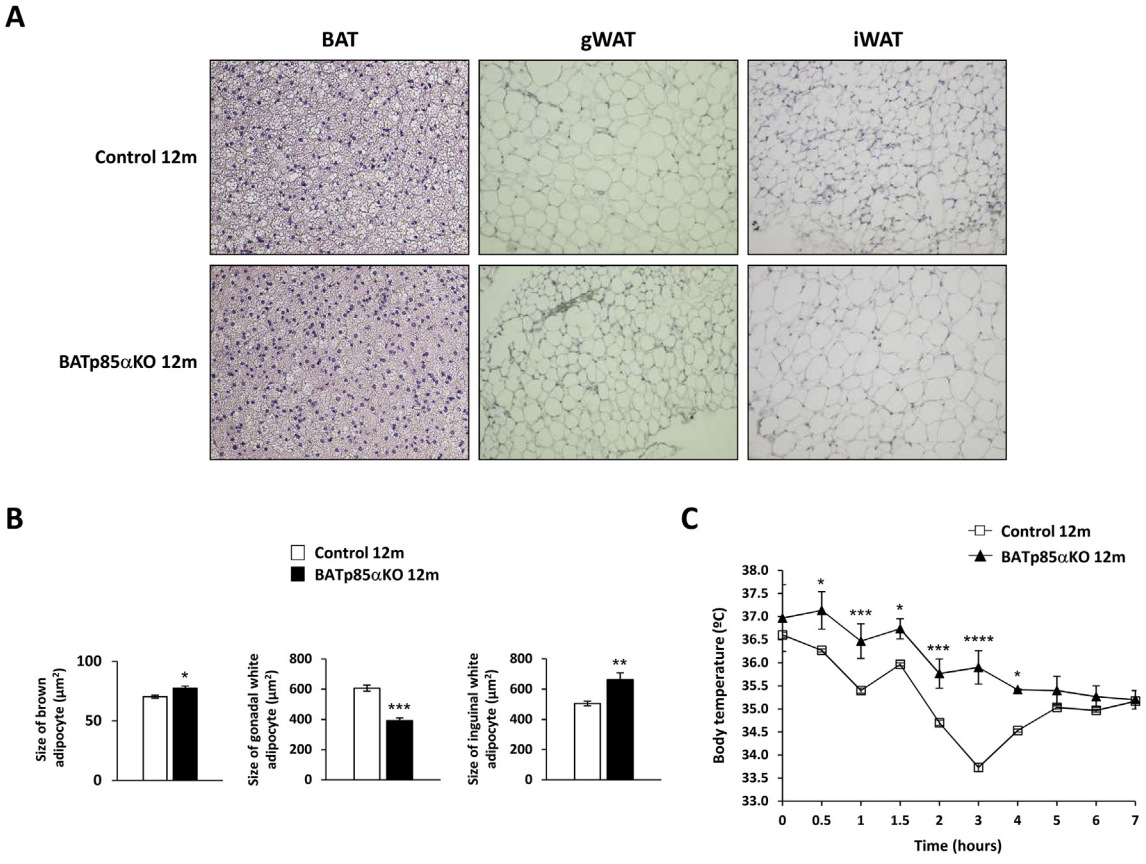

Figure 2: Characterization of BATp85αKO mice at 6 and 12 months of age. (A) Representative microphotographs of BAT, gWAT, or iWAT, stained with hematoxylin and eosin, in control or BATp85αKO mice at 12 months of age. Image magnification: 20 × . **(B)** Size quantification of brown or white adipocytes from control and BATp85αKO mice at 12 months of age. **(C)** Graph of body temperature at different times to analyze the thermogenic response to cold exposure in control and BATp85αKO mice at 12 months of age. Results are expressed as mean ± SEM. Statistical significance was assessed by two-tailed unpaired *t*-test by comparison with control 12-month-old mice (*$p < 0.05$, **$p < 0.01$, ***$p < 0.001$, and ****$p < 0.0001$). Twelve-month-old control (n = 10); 12-month-old BATp85αKO (n = 6). (For interpretation of the references to color in this figure legend, the reader is referred to the Web version of this article.)

2.10. Statistical analysis

All values are expressed as mean ± standard error of the mean (SEM). Differences between the two groups were assessed using unpaired two-tailed *t*-tests for experimental models. Data involving more than two groups were analyzed using a one-way analysis of variance (ANOVA) followed by Bonferroni and Tukey tests if differences were noted. Data involving two groups with two variables were analyzed using two-way ANOVA followed by a Sidak test if differences were noted (GraphPad Prism 6.0). The null hypothesis was rejected when $p < 0.05$.

3. RESULTS

3.1. Characterization of BATp85αKO mice

First, we genotyped control and BATp85αKO mice with two different PCRs (Figure 1A). BATp85αKO ($p85\alpha^{loxP/loxP}$; UCP-1-Cre recombinase^{+}) showed a unique band of 460 bp in the PCR of $p85\alpha^{loxP/loxP}$ (upper panel of Figure 1A) and two bands of 600 and 285 bp corresponding to Cre-recombinase and UCP-1, respectively (lower panel of Figure 1A). However, the control group showed a 460-bp band in $p85\alpha^{loxP/loxP}$; UCP-1-Cre recombinase^{-} mice and a 270-bp band in WT mice (upper panel, Figure 1A). In the second PCR, WT and $p85\alpha^{loxP/loxP}$; UCP-1-Cre recombinase^{-} mice showed only the band of 285 bp because both do not express Cre-recombinase (Figure 1A). In addition, we checked that the exon 7 of p85α was deleted in BAT from BATp85αKO mice as compared with control mice by PCR (Figure 1B) and by immunohistochemistry against p85α (Figure 1C and Supplemental Fig. 1).

The characterization of the BATp85αKO model was performed at 6 and 12 months of age. No significant differences were observed in body weight, BAT mass, or most of the vWAT compartments between control and BATp85αKO mice (Supplemental Fig. 2). In addition, several compartments of the adipose organ were characterized with hematoxylin-eosin staining, and the size of the adipocytes was quantified. It was observed that the loss of p85α in BAT significantly reduced the size of the gonadal white adipocytes, whereas the size of

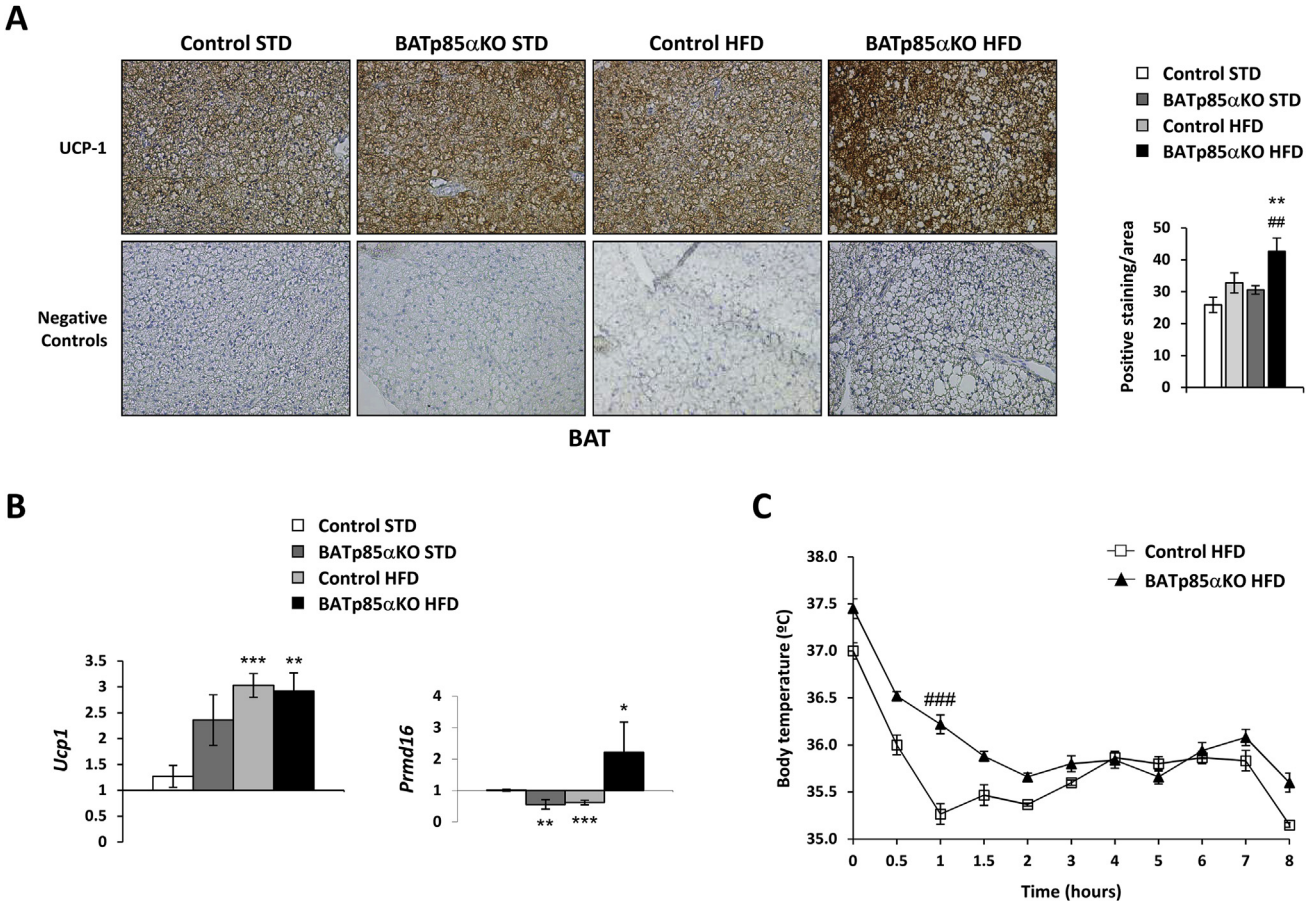

Figure 3: Brown fat functionality in BATp85αKO mice under HFD. (A) Representative microphotographs and quantification of UCP-1 protein in BAT from control and BAT-p85αKO mice by immunohistochemistry. **(B)** qRT-PCR analysis of *Ucp1* and *Prdm16* mRNA levels in BAT from the different groups studied. Thus, the amount of target, normalized to endogenous gene and relative to the control, is given by qRT-PCR. The value represented on the *y* axis is the RQ, being: [(RQ) $= 2^{-\Delta\Delta Ct}$; ΔCt (cycle threshold) = Ct (target gene) − Ct (*Gapdh*); ΔΔCt = ΔCt for any sample − ΔCt for the control]. Amplification of *Gapdh* was used in the same reaction of all samples as an internal control. We have used ΔΔCt referred to control STD. **(C)** Graphs of body temperature at different times (0−8 h, each hour) to analyze the thermogenic response to cold exposure from control and BATp85αKO mice under an HFD. Results are expressed as mean ± SEM. Statistical significance was carried out by one-way ANOVA with Bonferroni and Tukey post tests in B and C and two-tailed unpaired *t*-test in D by comparison with the control STD group (*$p < 0.05$, **$p < 0.01$, and ***$p < 0.001$) and with the control HFD group (##$p < 0.01$ and ###$p < 0.001$). Control STD (n = 5); control HFD (n = 8); BATp85αKO STD (n = 5); BATp85αKO HFD (n = 7). (For interpretation of the references to color in this figure legend, the reader is referred to the Web version of this article.)

the inguinal white and brown adipocytes were larger with respect to the control group at 6 and 12 months of age (Supplemental Fig. 3 and Figure 2A, B, respectively).

To assess the thermogenic function of BAT with or without p85α, 12-month-old control and BATp85αKO mice underwent a cold adaptation experiment. Our results showed that the lack of p85α in BAT induced a better cold adaptation because in most of the time points studied, the rectal temperature was maintained at 1° higher than that of the control group (Figure 2C).

We also studied the impact on glucose metabolism of the lack of p85α in BAT. In this regard, glucose and insulin tolerance tests showed similar profiles in both groups at 6 and 12 months of age, respectively (Supplemental Fig. 4).

To challenge the thermogenic capacity of control and BATp85αKO mice, an HFD was administered to evaluate their susceptibility or resistance to developing obesity. Thus, we observed a significant increase in UCP-1 expression in the BATp85αKO versus control mice as assayed by immunohistochemistry (Figure 3A). In addition, *Prdm16*, a specific marker of brown adipogenesis, was also increased in BATp85αKO as compared with control mice under an HFD (Figure 3B). These facts might explain the better adaptation of BATp85αKO HFD to cold exposure at the different time points studied as compared with the control HFD group (Figure 3C).

3.2. Lack of p85α in BAT confers obesity resistance

If we compare both groups under a HFD, we can see that body weight and the ratio of different compartments of the adipose organ/body weight were significantly diminished in the BATp85αKO mice (Figure 4A, B and C). Moreover, BATp85αKO showed a smaller increase in body weight gain, a significant decrease in body weight after 10 weeks of an HFD, and no significant changes in food intake per week as compared with the control HFD group (Supplemental Figs. 5A, B, and C). In addition, BATp85αKO versus control mice showed a significantly lower fat body content as measured by NMR (Figure 5A). In addition, we studied brown, gonadal, and inguinal cell size in both groups of mice. As expected, the adipocyte size in all of the studied compartments was significantly increased in control mice fed an HFD. In BATp85αKO mice, we observed a lower increase in the adipocyte size as compared with the controls under an HFD (Figure 4D).

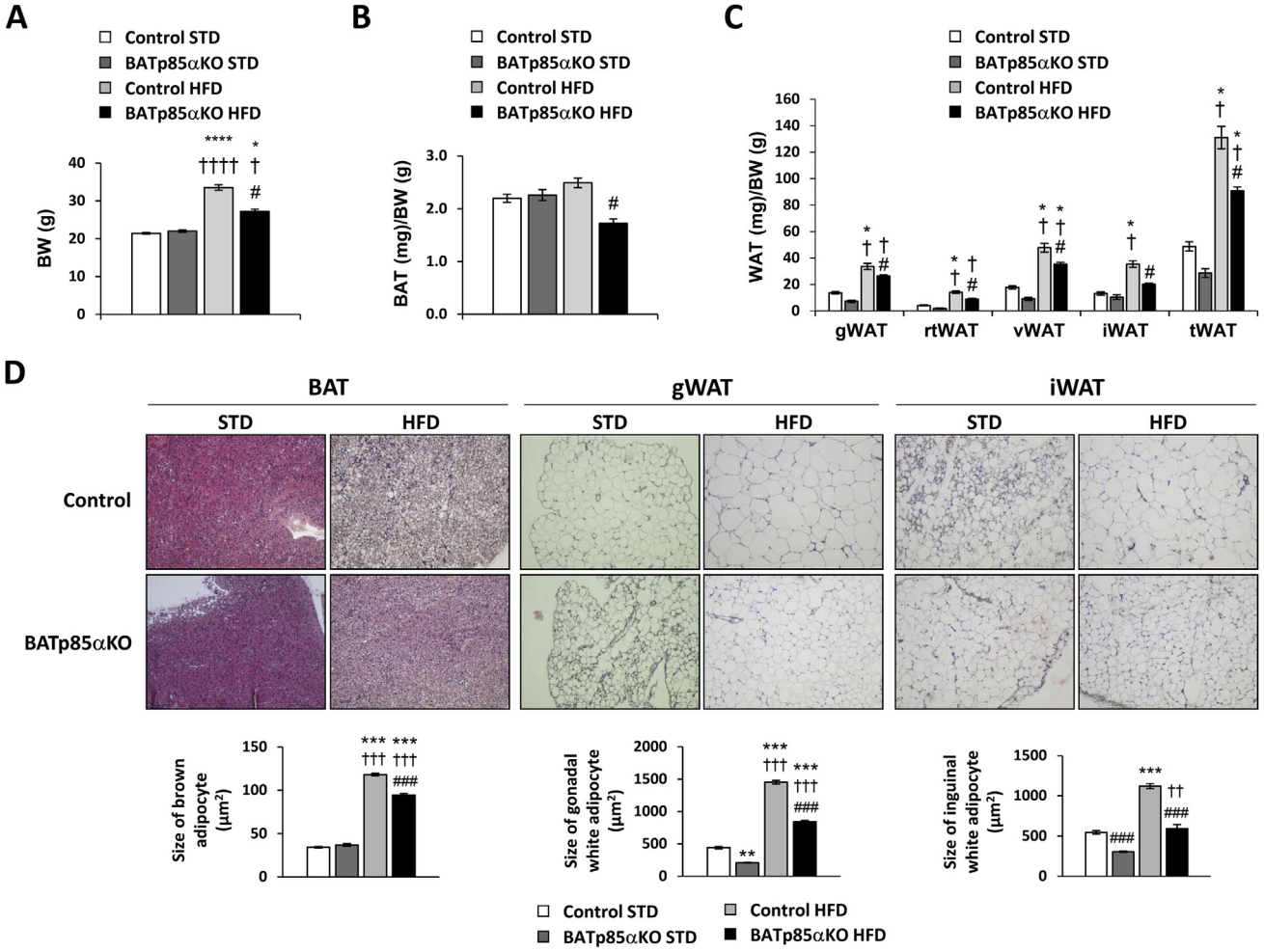

Figure 4: The lack of p85α in BAT reduces obesity and adipocyte size. (A) Body weight (BW) (g), **(B)** BAT (mg)/BW (g) ratio, and **(C)** WAT (mg)/BW (g) ratio from control STD, BATp85αKO STD, control HFD, and BATp85αKO HFD groups. **(D)** Representative microphotographs and quantification of BAT, gWAT, or iWAT stained with hematoxylin and eosin from control and BATp85αKO HFD groups. Image magnification: 20×. Control STD (n = 5); control HFD (n = 8); BATp85αKO STD (n = 5); BATp85αKO HFD (n = 7). Results are expressed as mean ± SEM. Statistical significance was carried out by one-way ANOVA with Bonferroni and Tukey posttests by comparison with control STD mice (*$p < 0.05$, **$p < 0.01$, ***$p < 0.001$, and ****$p < 0.0001$), with BATp85αKO STD mice (†$p < 0.05$, ††$p < 0.01$, †††$p < 0.001$, and ††††$p < 0.0001$), and with control HFD mice (#$p < 0.05$ and ###$p < 0.001$).

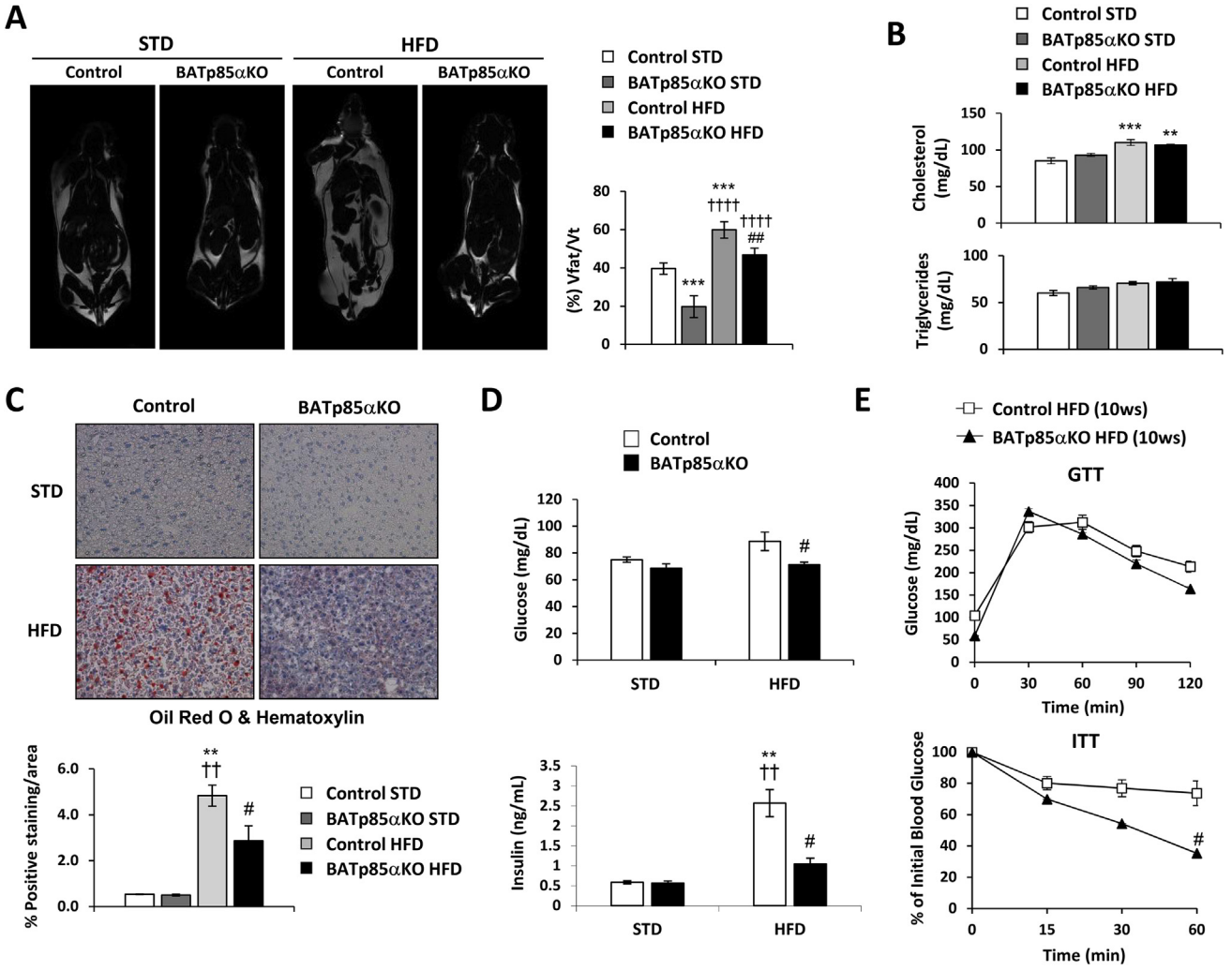

Figure 5: The lack of p85α in BAT reduces obesity, fatty liver, and insulin resistance. (A) Representative nuclear magnetic resonance images from the four groups studied to assess the percentage of fat volume versus total volume. **(B)** Plasma cholesterol and triglyceride levels from the four groups studied. **(C)** Representative microphotographs and quantification of livers stained with Oil Red O contrasted with hematoxylin to identify lipid depots. Image magnification: 10 × . **(D)** Glucose and insulin plasma levels of fasted mice by automatic monitor or by ELISA, respectively. **(E)** Glucose tolerance test (GTT) (upper) and insulin tolerance test (ITT) (lower) after 10 weeks on an HFD were performed in control HFD and BATp85αKO HFD nice. Control STD (n = 5); control HFD (n = 8); BATp85αKO STD (n = 5); BATp85αKO HFD (n = 7). Results are expressed as mean ± SEM. Statistical significance was carried out by one-way ANOVA with Bonferroni and Tukey posttests in A, B, and C; two-way ANOVA with Sidak posttest in D; and two-tailed unpaired *t*-test in E by comparison with the control STD group (*$p < 0.05$, **$p < 0.01$, and ***$p < 0.001$), with the BATp85αKO STD group (††$p < 0.01$ and ††††$p < 0.0001$), and with the control HFD group (#$p < 0.05$ and ##$p < 0.01$). Male mice were sacrificed at 16 weeks. (For interpretation of the references to color in this figure legend, the reader is referred to the Web version of this article.)

3.3. Lack of p85α in BAT improves fatty liver and insulin resistance

The analysis of cholesterol levels revealed an increase in those mice subjected to HFD, and this change was significantly higher in control than in BATp85αKO mice. However, plasma triglyceride levels were similar in both groups under an HFD (Figure 5B). In addition, with the Oil Red O stain, we found that the BATp85αKO group has a significantly lower lipid accumulation in the liver in relation to the control HFD group (Figure 5C).

A significantly lower fasting basal glucose was found in BATp85αKO as compared with control mice under an HFD (Figure 5D). More importantly, in control mice under an HFD, insulin resistance was revealed as the compensatory hyperinsulinemia (Figure 5D). However, BATp85αKO mice showed no compensatory hyperinsulinemia under an HFD, suggesting increased insulin sensitivity (Figure 5D). To assess the metabolic status of control and BATp85αKO mice, glucose and insulin tolerance tests were performed. BATp85αKO mice showed a similar glucose tolerance as controls after 10 weeks on an HFD (Figure 5E). At the fifth week, both groups showed normal insulin sensitivity, as revealed by the insulin tolerance test (Supplemental Fig. 5D). However, at 10 weeks, control mice showed a severe insulin resistance, whereas BATp85αKO mice showed normal insulin sensitivity (Figure 5E).

3.4. Mechanisms implicated in the improvement of obesity and metabolic complications in BATp85αKO mice

To assess the contribution of the adipose depots to the overall insulin resistance, we performed *in vivo* insulin-signaling studies, checking for Akt phosphorylation in response to insulin in BAT, gWAT, and iWAT. Insulin-induced Akt phosphorylation in these tissues was significantly

improved in BATp85αKO mice under an HFD as compared with controls (Figure 6A). In addition, we analyzed the phosphorylation of JNK, a well-known mediator of insulin resistance. A significant decrease in JNK phosphorylation was observed in BAT from BATp85αKO HFD mice as compared with controls (Figure 6B).

In a further step, we also analyzed whether p85α deletion might modify the profile of IR isoform expression, its association with IRS-1, and, consequently, the insulin signaling. Thus, we observed that the lack of p85α significantly increased IRB levels (Figure 6C, E) and the association with IRS-1 (Figure 6C). However, the expression of IRA or IGF-1R was very similar between both groups (Figure 6C, D and E).

As HFD-induced obesity enhances the expression of proinflammatory molecules, triggering the local and global inflammatory processes that contribute to the onset of peripheral insulin resistance and its associated metabolic complications, we analyzed by qRT-PCR the mRNA levels of *Tnfa*, *Leptin*, and *Adipoq* in BAT, gWAT, and iWAT from the control and BATp85αKO mice under an HFD. *Tnfa* mRNA expression was significantly increased in the three adipose depots studied in control mice under an HFD versus STD. However, their levels were significantly decreased in BATp85αKO mice as compared with control mice under an HFD (Figure 7). *Leptin* mRNA expression remained unchanged in BAT, whereas its expression was lower in iWAT or gWAT

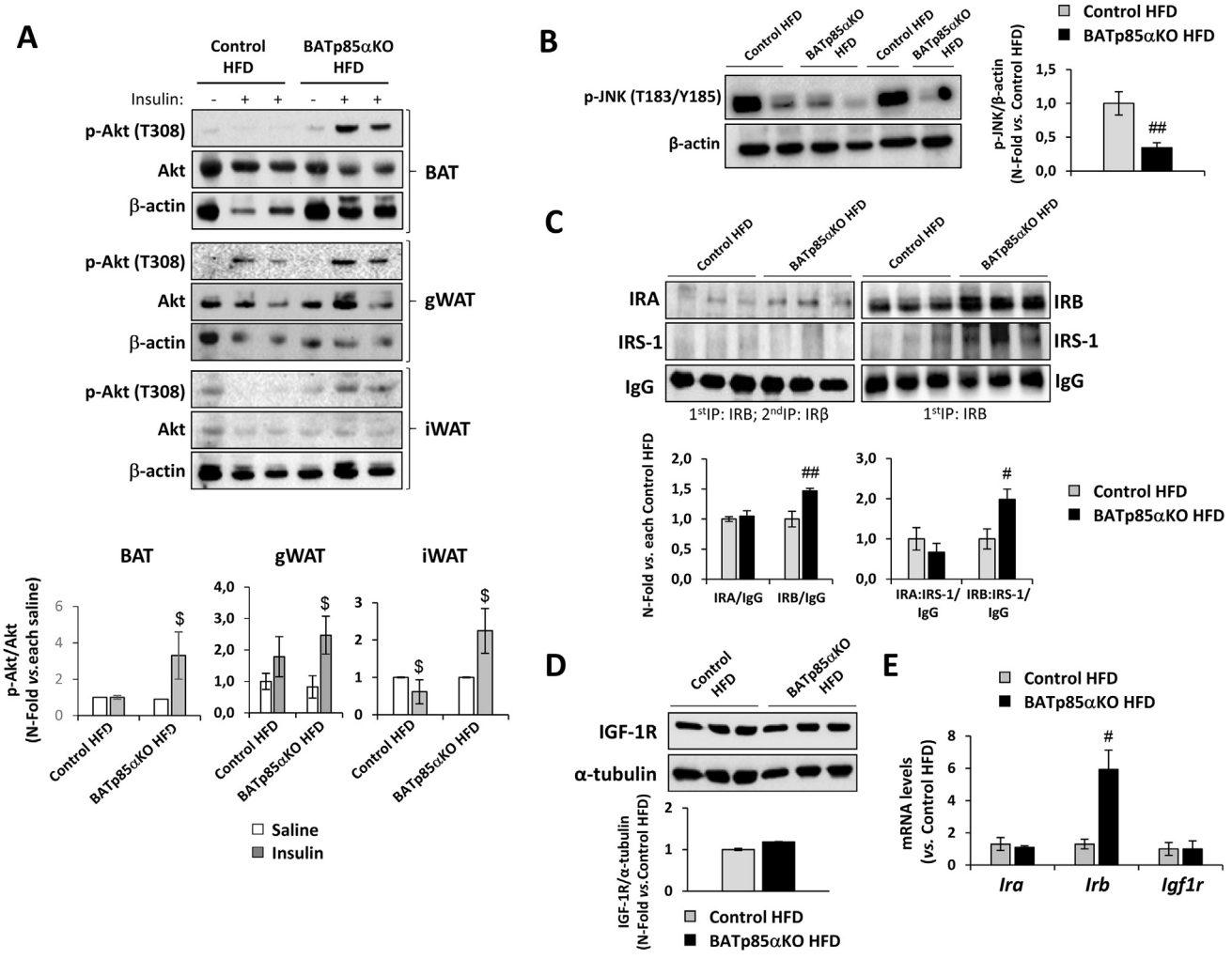

Figure 6: The lack of p85α in BAT improves insulin signaling in adipose depots through a lower JNK activation and a higher IRB expression. (A) Western blot analysis of Akt phosphorylation in response to insulin in control versus BATp85αKO mice fed an HFD. Representative gels and quantification of *in vivo* insulin signaling studies performed in both groups after 10 weeks on an HFD. In BAT: control HFD (n = 7, with saline [n = 2] and with insulin [n = 5]), BATp85αKO HFD (n = 6, with saline [n = 2] and with insulin [n = 4]); in gWAT: control HFD (n = 7, with saline [n = 3] and with insulin [n = 4]), BATp85αKO HFD (n = 7, with saline [n = 3] and with insulin [n = 4]); and in iWAT: control HFD (n = 7, with saline [n = 2] and with insulin [n = 5]), BATp85αKO HFD (n = 8, with saline [n = 2] and with insulin [n = 6]). **(B)** Representative gels and quantification of JNK phosphorylation (T183/Y185) by Western blot of BAT from control HFD and BATp85αKO HFD mice. β-actin was used as a loading control. Control HFD (n = 6); BATp85αKO HFD (n = 7). **(C)** Representative gels and quantifications of IRA (left panels) and IRB (right panels) protein levels and their association with IRS-1 in BAT from control and BATp85αKO HFD mice. Control HFD (n = 6–9); BATp85αKO HFD (n = 6–9). **(D)** Representative gels and quantification of the IGF-1R by Western blot of BAT from control or BATp85αKO mice under HFD. α-tubulin was used as a loading control. Control HFD (n = 3); BATp85αKO HFD (n = 3). **(E)** *Ira*, *Irb*, and *Igf1r* mRNA levels were analyzed by qRT-PCR in BAT from control HFD and BATp85αKO HFD. Control HFD (n = 8); BATp85αKO HFD (n = 7). Results are expressed as mean ± SEM. Statistical significance was performed by two-way ANOVA with Sidak posttest in A and two-tailed unpaired *t*-test in B, C, D, and E by comparison with each group with saline ($$p < 0.05$); and with the control HFD group (#$p < 0.05$ and ##$p < 0.01$).

in BATp85αKO as compared with control mice under an HFD (Figure 7B). Conversely, *Adipoq* mRNA levels were significantly increased in gWAT in BATp85αKO as compared with control mice (Figure 7C). In addition, we also measured the mRNA levels of *Mcp1*, *Il1b*, and *Il6* in BAT and iWAT from both groups under an HFD. BATp85αKO mice showed a significant decrease in *Il6* expression in iWAT as compared with control HFD mice (Supplemental Fig. 6).

Finally, we studied the contribution of white fat browning to the overall HFD-induced obesity in the BATp85αKO mice. Thus, we assessed UCP-1 levels by several techniques (qRT-PCR, immunohistochemistry, and Western blot) and the expression of *Prdm1*6 by qRT-PCR. The expression of UCP-1 at protein or mRNA levels and *Prdm16* at the mRNA level was significantly decreased in control mice under an HFD as compared with an STD (Figure 8A, B, and D). However, the loss of *Ucp1* or *Prdm16* expression was precluded in BATp85αKO mice as compared with controls under an HFD (Figure 8). Moreover, we observed a significant increase in AMPK activation by phosphorylation in the residue T172 and its total protein levels (Figure 8C), which might explain the higher UCP-1 protein levels observed in iWAT from BATp85αKO HFD as compared with control HFD mice (Figure 8B).

4. DISCUSSION

In the past decade, the importance of BAT in humans and its contribution to the prevention of obesity have been established [4–7]. Therefore, to explore potential antiobesity drugs, better knowledge about BAT activity regulation is required [21]. Previously, the ability of BAT thermogenic function to protect against obesity in animal models lacking BAT or UCP-1 was demonstrated [22]. In fact, previous studies carried out in Brown Adipose Tissue Insulin Receptor KnockOut (BATIRKO) mice, a mouse model showing severe brown lipoatrophy, demonstrated a susceptibility to obesity together with metabolic and vascular alterations [19,20,23]. In addition, individuals with a lower amount of functional BAT are more prone to an increase in body weight, with an inverse relationship between BAT levels and body mass index [5].

The current work has been committed to generating a new mouse model that shows enhanced brown fat thermogenic functionality that is reluctant to develop obesity under an HFD. In fact, BATp85αKO showed better cold adaptation as compared with control mice. An association was previously described between the gain of BAT function

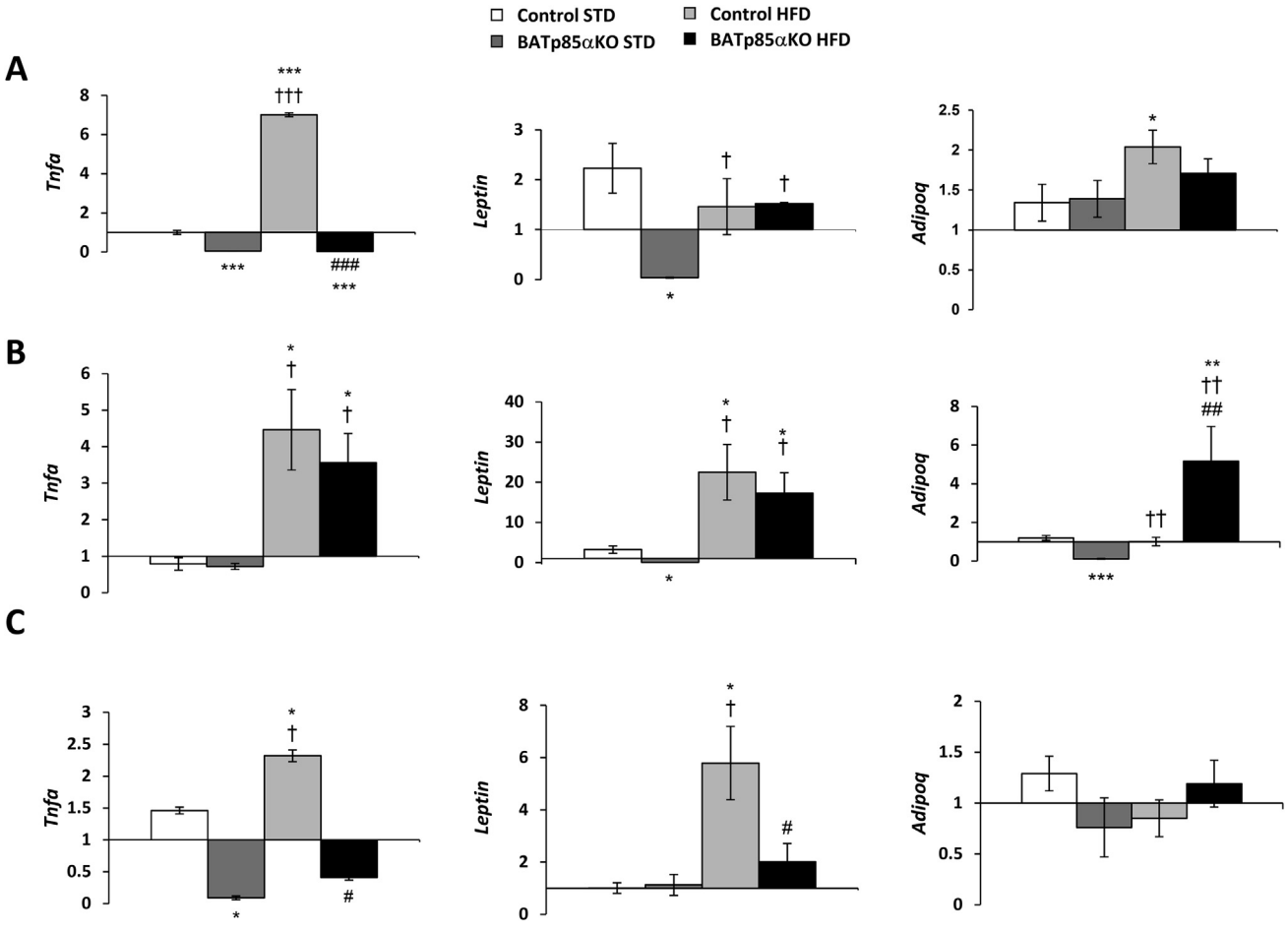

Figure 7: The lack of p85α in BAT modified the expression profile of adipokines in the adipose organ. *Tnfa*, *Leptin*, or *Adipoq* mRNA levels were analyzed by qRT-PCR in **(A)** BAT, **(B)** gWAT, and **(C)** iWAT from the four groups studied. Thus, the amount of target, normalized to endogenous gene and relative to the control, is given by qRT-PCR. The value represented on the *y* axis is the RQ, being: [(RQ) = $2^{-\Delta\Delta Ct}$; ΔCt (cycle threshold) = Ct (target gene) − Ct (*Gapdh*); ΔΔCt = ΔCt for any sample − ΔCt for the control]. Amplification of *Gapdh* was used in the same reaction of all samples as an internal control. We have used ΔΔCt referred to control STD. Results are expressed as mean ± SEM. Statistical significance was assessed by one-way ANOVA with Bonferroni and Tukey posttests by comparison with control STD mice (*$p < 0.05$, **$p < 0.01$, and ***$p < 0.001$), with BATp85αKO STD mice (†$p < 0.05$, ††$p < 0.01$, and †††$p < 0.001$), and with control HFD mice (#$p < 0.05$, ##$p < 0.01$, and ###$p < 0.001$). Control STD (n = 5); control HFD (n = 8); BATp85αKO STD (n = 5); BATp85αKO HFD (n = 7).

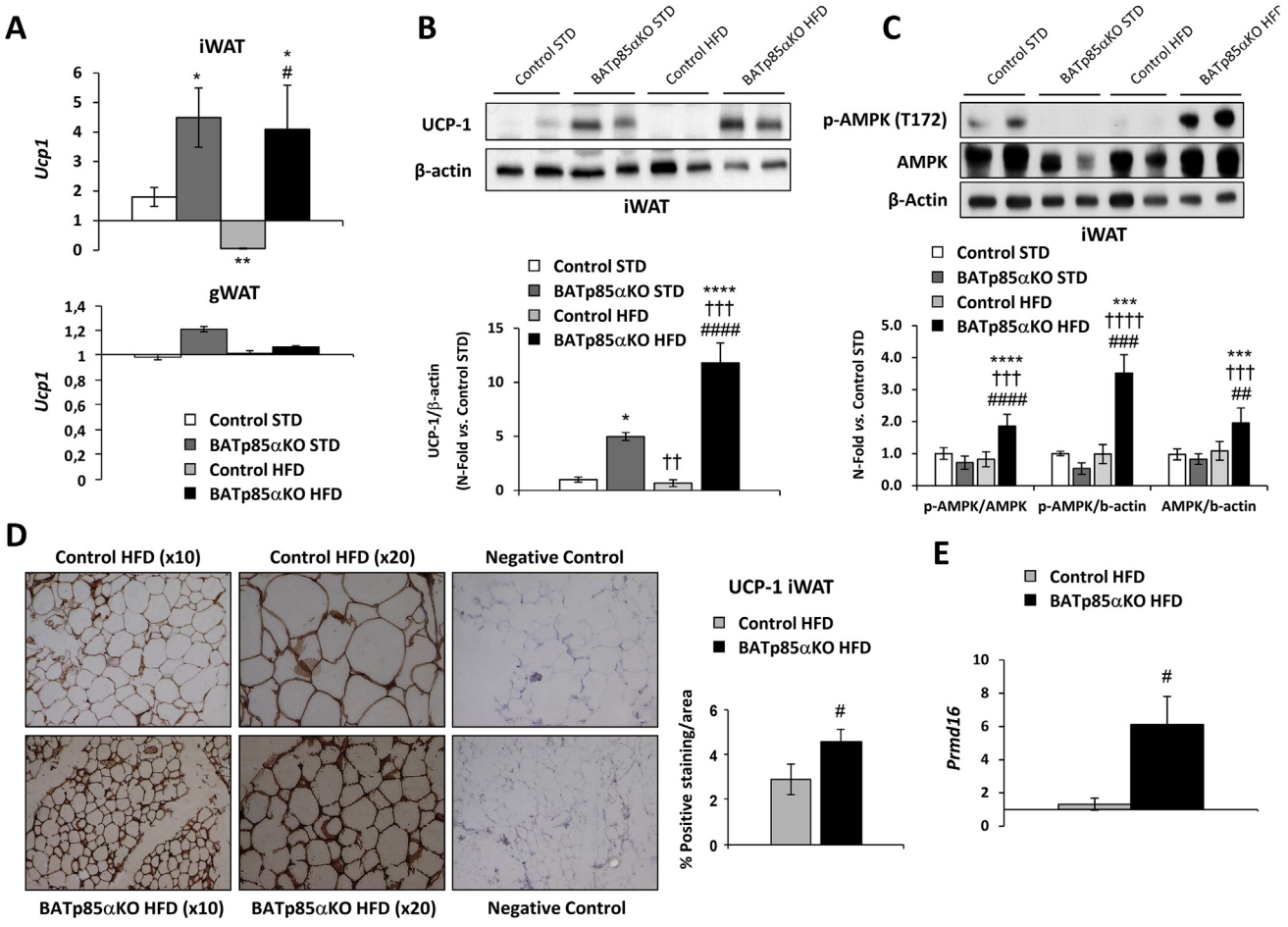

Figure 8: The lack of p85α in BAT might induce iWAT browning. (A) Analysis of *Ucp1* mRNA levels in gWAT or iWAT from the four groups studied by qRT-PCR. *Gapdh* was used as an endogenous target. The value represented on the *y* axis is the RQ and is referred to control STD. Western blot analysis of **(B)** UCP-1 and **(C)** p-AMPK protein levels in iWAT from the four groups studied. **(D)** Representative microphotographs and their quantification of UCP-1 protein by immunohistochemistry in iWAT from control HFD and BATp85αKO HFD mice. Image magnification: 10× and 20×. **(E)** Analysis of *Prdm16* mRNA levels in iWAT from control HFD and BATp85αKO HFD mice by qRT-PCR. *Gapdh* was used as an endogenous target. The value represented on the *y* axis is the RQ and is referred to control HFD. Results are expressed as mean ± SEM. Statistical significance was carried out by one-way ANOVA with Bonferroni and Tukey post tests in A, B, and C and two-tailed unpaired *t*-test in D and E by comparison with control STD mice (*$p < 0.05$, **$p < 0.01$, ***$p < 0.001$, and ****$p < 0.0001$), with BATp85αKO STD mice (††$p < 0.01$, †††$p < 0.001$, and ††††$p < 0.0001$) and with control HFD mice (#$p < 0.05$, ##$p < 0.01$, ###$p < 0.001$, and ####$p < 0.0001$). Control STD (n = 5); control HFD (n = 8); BATp85αKO STD (n = 5); BATp85αKO HFD (n = 7).

and better cold adaptation in experimental models [24–27] as well as in humans [28,29]. Mice or patients with obesity showed worse thermogenic adaptation to cold and less BAT activity [24,30]. In addition, cold exposure is a useful intervention for improving thermogenic capacity [26–29]. In our mouse model, we described that the loss of p85α in BAT improved its functionality, which was associated with an increased *Ucp1* or *Prdm16* mRNA expression. In this regard, both proteins have been previously described as essential for the thermogenic activity of BAT, and their ablation caused metabolic dysfunction and obesity [22,31].

Our results demonstrate a significant decrease in body weight and total fat accumulation without changes in food intake as well as a decrease in the size of both white and brown adipocytes in BATp85αKO versus control mice under an HFD. In this regard, previous studies have described an increased adipose cell number with normal or increased size in obesity models [32]. Moreover, a saturated fatty acid diet was significantly correlated with increased fat cell size and number, establishing a relationship between fat cell size and number and fatty acid composition in adipose tissue from different fat depots in humans with overweight/obesity [33].

Obesity is also associated with a spectrum of liver abnormalities, known as nonalcoholic fatty liver disease, characterized by an increase in intrahepatic triglyceride content with or without inflammation and fibrosis [34,35]. Our BATp85αKO mouse model, as compared with control mice, showed a marked reduction in obesity together with lower plasma cholesterol levels and nonhepatic steatosis. In this regard, excessive intrahepatic triglyceride content in individuals with obesity is a robust marker of metabolic abnormalities [34]. Moreover, initial studies suggested that BAT activation in humans and experimental models may also reduce triglyceride and cholesterol levels [35,36] and improve glucose uptake through GLUT-1 and GLUT-4 transporters [37,38].

Regarding the mechanisms underlying the reduction of obesity demonstrated in BATp85αKO versus control mice under an HFD, different models have been described that bear a deletion of distinct PI3K subunits that gave rise to a wide range of metabolic

phenotypes. The deletion of p110α, but not p110β, in the adipose organ was associated with marked effects on basal BAT respiration and produced a whole-body phenotype similar to that observed in metabolic syndrome [39]. On the other hand, mice carrying a dominant-negative human PI3K mutation are protected from obesity and hepatic steatosis but not insulin resistance and diabetes [40]. In contrast, despite the critical role of PI3Ks in insulin signaling, mice with heterozygous deletion of p85α or loss of p85β have paradoxically improved PI3K activity and increased insulin sensitivity [14–16], at least in part owing to an improved balance between p85-p110 dimer and monomeric p85 competing for binding to phosphorylated IRS-1 and IRS-2 [41]. In our model, the lack of p85α in BAT increased insulin signaling in this tissue and also in visceral and subcutaneous WATs. One important mechanism involved in obesity-linked insulin resistance is the stress kinase JNK [42]. Several studies have described that the p85 regulatory subunit is required for the activation of JNK by insulin or endoplasmic reticulum stress stimuli (obesity and chemical agents). In addition to its traditional positive functions in the PI3K pathway, p85 acts as a negative regulator of insulin signaling via a JNK-mediated negative feedback loop [43]. In this regard, a significant decrease in JNK activation was noted in BAT from BATp85αKO as compared with control mice under an HFD. An alternative mechanism that might affect the insulin sensitivity is the variation in the IR isoforms' expression profile and their association with IRSs. Changes have been described in the expression profile of IR isoforms in several diseases, such as insulin resistance, cancer, and atherosclerosis affecting insulin signaling and favoring the proliferation or apoptosis in certain type of cells [20,44–46]. In BAT, we observed a significant increase in IRB protein levels and its association with IRS-1, which may contribute to the observed improvement in the insulin signaling in BATp85αKO compared with control mice under HFD.

We previously described that brown fat lipoatrophy and increased visceral adiposity through concerted adipocytokines overexpression induced insulin resistance and vascular dysfunction [18]. To address this important issue, we studied the expression of proinflammatory adipocytokines in the adipose depots that is perhaps responsible for a local inflammatory effect that may account for the differential insulin resistance observed in BATp85αKO versus control mice under an HFD. In this sense, we observed a concerted decreased expression of insulin resistance inducers such as *Tnfa* or *Leptin* in BAT, gWAT, or iWAT in BATp85αKO versus control mice under an HFD. However, a significant increase in adiponectin in gWAT depots was observed under the same experimental conditions. It is noteworthy that changes in adipose tissue are associated with systemic arterial dysfunction and insulin resistance, suggesting that adipose inflammation may be linked to insulin resistance in subjects with obesity [47].

Finally, another mechanism involved in the overall susceptibility or resistance to obesity is the browning effect on the adipose organ and particularly on the inguinal white fat depots. In this regard, we show a significant increase in *Ucp1* mRNA levels and positive immunostaining or in *Prdm16* mRNA levels in iWAT from BATp85αKO versus control mice under an HFD. At the molecular level, it has been previously described that browning in the adipose organ is regulated by multiple factors and signaling pathways. In this sense, PPARγ is a master regulator of mitochondrial biogenesis and oxidative metabolism in adipocytes that induce the expression of UCP-1 and other thermogenic components such as Prdm16d, which are involved in brown adipogenesis within the white depots [48,49]. On the other hand, AMPK is a critical regulator of adipose energy metabolism [50], and its AMPKα isoform plays a key role in brown adipogenesis [51]. It has been recently described that both resveratrol and phytol are capable of inducing iWAT browning through AMPKα in mice fed an HFD [52–54]. According to these results, elevated AMPK levels and its phosphorylated form together with a significant increase in UCP-1 and Prdm16 expression were noted in iWAT from BATp85αKO mice under an HFD as compared with controls.

5. CONCLUSIONS

In conclusion, our data strongly suggest that under an HFD, the loss of p85α in BAT improves thermogenic functionality, inducing obesity resistance as visualized by increased insulin sensitivity and a nonfatty liver. The reluctance of BATp85αKO mice to develop obesity under an HFD was related to 1) increased IRB/IRS-1 association and insulin signaling, 2) decreased JNK activation 3), lower levels of proinflammatory adipocytokines and higher levels of adiponectin in the iWAT or gWAT, and 4) increased iWAT browning.

FUNDING

This work was supported by grants SAF2014/51795-R and SAF2017-82133-R from Ministerio de Ciencia e Innovación, Comunidad de Madrid (B2017/BMD-3684) and ISCIII (PIE14/00061) given to M. Benito, and CIBER de Diabetes y Enfermedades Metabólicas Asociadas (CIBERDEM). ARL-P was funded by Programa Operativo de Empleo Juvenil from Comunidad de Madrid.

AUTHOR CONTRIBUTIONS

A.G.-H. participated in the acquisition, analysis, and interpretation of data as well as in the design and coordination of the study and wrote the manuscript. C.R.-L., P.M., O.E., A.R. L.-P., N.B., V.V.-H., M.L.-H., and G.S. participated in the acquisition, analysis, and interpretation of data. S.F. and G.G.-G. developed both murine experimental models. M.B. participated in the design and review of the manuscript. All authors discussed the results and approved the final manuscript.

CONFLICTS OF INTEREST

None declared.

APPENDIX A. SUPPLEMENTARY DATA

Supplementary data to this article can be found online at https://doi.org/10.1016/j.molmet.2019.10.010.

REFERENCES

[1] GBD 2015 Maternal Mortality Collaborators. Global, regional, and national levels of maternal mortality, 1990-2015: a systematic analysis for the Global Burden of Disease Study 2015. Lancet 388(10053), 2016:1775–1812.

[2] Mathieu, P., Lemieux, I., Després, J.P., 2010. Obesity, inflammation, and cardiovascular risk. Clinical Pharmacology & Therapeutics 87:407–416.

[3] Gesta, S., Tseng, Y.H., Kahn, C.R., 2007. Developmental origin of fat: tracking obesity to its source. Cell 131:242–256.

[4] Cannon, B., Nedergaard, J., 2004. Brown adipose tissue: function and physiological significance. Physiological Reviews 84:277–359.

[5] Cypess, A.M., Lehman, S., Williams, G., Tal, I., Rodman, D., Goldfine, A.B., et al., 2009. Identification and importance of brown adipose tissue in adult humans. New England Journal of Medicine 360:1509–1517.

[6] Bartelt, A., Bruns, O.T., Reimer, R., Hohenberg, H., Ittrich, H., Peldschus, K., et al., 2011. Brown adipose tissue activity controls triglyceride clearance. Nature Medicine 17:200–205.

[7] Stanford, K.I., Middelbeek, R.J., Townsend, K.L., An, D., Nygaard, E.B., Hitchcox, K.M., et al., 2013. Brown adipose tissue regulates glucose homeostasis and insulin sensitivity. Journal of Clinical Investigation 123: 215–223.

[8] Engelman, J.A., Luo, J., Cantley, L.C., 2006. The evolution of phosphatidylinositol 3-kinases as regulators of growth and metabolism. Nature Reviews Genetics 7:606e19.

[9] Vanhaesebroeck, B., Guillermet-Guibert, J., Graupera, M., Bilanges, B., 2010. The emerging mechanisms of isoform-specific PI3K signalling. Nature Reviews Molecular Cell Biology 11:329e41.

[10] Dhand, R., Hara, K., Hiles, I., Bax, B., Gout, I., Panayotou, G., et al., 1994 Feb 1. PI 3-kinase: structural and functional analysis of intersubunit interactions. The EMBO Journal 13(3):511–521.

[11] Gout, I., Dhand, R., Panayotou, G., Fry, M.J., Hiles, I., Otsu, M., et al., 1992. Expression and characterization of the p85 subunit of the phosphatidylinositol 3-kinase complex and a related p85 beta protein by using the baculovirus expression system. Biochemical Journal 288(Pt 2):395–405.

[12] Hirsch, E., Costa, C., Ciraolo, E., 2007. Phosphoinositide 3-kinases as a common platform for multi-hormone signaling. Journal of Endocrinology 194: 243e56.

[13] Beretta, M., Bauer, M., Hrisch, E., 2015. PI3K signaling in the pathogenesis of obesity: the cause and the cure. Advances in biological regulation 58:1–15.

[14] Terauchi, Y., Tsuji, Y., Satoh, S., Minoura, H., Murakami, K., Okuno, A., et al., 1999. Increased insulin sensitivity and hypoglycaemia in mice lacking the p85 alpha subunit of phosphoinositide 3-kinase. Nature Genetics 21:230–235.

[15] Mauvais-Jarvis, F., Ueki, K., Fruman, D.A., Hirshman, M.F., Sakamoto, K., Goodyear, L.J., et al., 2002. Reduced expression of the murine p85alpha subunit of phosphoinositide 3-kinase improves insulin signaling and ameliorates diabetes. Journal of Clinical Investigation 109:141–149.

[16] Ueki, K., Yballe, C.M., Brachmann, S.M., Vicent, D., Watt, J.M., Kahn, C.R., et al., 2002. Increased insulin sensitivity in mice lacking p85beta subunit of phosphoinositide 3-kinase. Proceedings of the National Academy of Sciences of the U S A 99:419–424.

[17] Luo, J., McMullen, J.R., Sobkiw, C.L., Zhang, L., Dorfman, A.L., Sherwood, M.C., et al., 2005. Class IA phosphoinositide 3-kinase regulates heart size and physiological cardiac hypertrophy. Molecular and Cellular Biology 25(21):9491–9502.

[18] Gómez-Hernández, A., Otero, Y.F., de las Heras, N., Escribano, O., Cachofeiro, V., Lahera, V., et al., 2012. Brown fat lipoatrophy and increased visceral adiposity through a concerted adipocytokines overexpression induces vascular insulin resistance and dysfunction. Endocrinology 153(3): 1242–1255.

[19] Gómez-Hernández, A., Beneit, N., Escribano, Ó., Díaz-Castroverde, S., García-Gómez, G., Fernández, S., et al., 2016. Severe Brown fat lipoatrophy aggravates atherosclerotic process in male mice. Endocrinology 157:3517–3528.

[20] Escribano, O., Guillén, C., Nevado, C., Gómez-Hernández, A., Kahn, C.R., Benito, M., 2009. Beta-Cell hyperplasia induced by hepatic insulin resistance: role of a liver-pancreas endocrine axis through insulin receptor A isoform. Diabetes 58:820–828.

[21] Bhatt, P.S., Dhillo, W.S., Salem, V., 2017. Human brown adipose tissue - function and therapeutic potential in metabolic disease. Current Opinion in Pharmacology 37:1–9.

[22] Kontani, Y., Wang, Y., Kimura, K., Inokuma, K.I., Saito, M., Suzuki-Miura, T., et al., 2005. UCP1 deficiency increases susceptibility to diet-induced obesity with age. Aging Cell 4:147–155.

[23] Guerra, C., Navarro, P., Valverde, A.M., Arribas, M., Brüning, J., Kozak, L.P., et al., 2001. Brown adipose tissue-specific insulin receptor knockout shows diabetic phenotype without insulin resistance. Journal of Clinical Investigation 108:1205–1213.

[24] Poekes, L., Legry, V., Schakman, O., Detrembleur, C., Bol, A., Horsmans, Y., et al., 2017. Defective adaptive thermogenesis contributes to metabolic syndrome and liver steatosis in obese mice. Clinical Science 131: 285–296.

[25] Bal, N.C., Singh, S., Reis, F.C.G., Maurya, S.K., Pani, S., Rowland, L.A., et al., 2017. Both brown adipose tissue and skeletal muscle thermogenesis processes are activated during mild to severe cold adaptation in mice. Journal of Biological Chemistry 292:16616–16625.

[26] Mineo, P.M., Cassell, E.A., Roberts, M.E., Schaeffer, P.J., 2012. Chronic cold acclimation increases thermogenic capacity, non-shivering thermogenesis and muscle citrate synthase activity in both wild-type and brown adipose tissue deficient mice. Comparative Biochemistry and Physiology Part A: Molecular & Integrative Physiology 161:395–400.

[27] Lim, S., Honek, J., Xue, Y., Seki, T., Cao, Z., Andersson, P., et al., 2012. Cold-induced activation of brown adipose tissue and adipose angiogenesis in mice. Nature Protocols 7:606–615.

[28] Blondin, D.P., Labbé, S.M., Tingelstad, H.C., Noll, C., Kunach, M., Phoenix, S., et al., 2014. Increased brown adipose tissue oxidative capacity in cold-acclimated humans. The Journal of Cinical Endocrinology and Metabolism 99:E438–E446.

[29] Hanssen, M.J., van der Lans, A.A., Brans, B., Hoeks, J., Jardon, K.M., Schaart, G., et al., 2016. Short-term cold acclimation recruits Brown adipose tissue in obese humans. Diabetes 65(5):1179–1189.

[30] Pradhan, R.N., Zachara, M., Deplancke, B., 2017. A systems perspective on brown adipogenesis and metabolic activation. Obesity Reviews 18(Suppl 1): 65–81.

[31] Cohen, P., Levy, J.D., Zhang, Y., Frontini, A., Kolodin, D.P., Svensson, K.J., et al., 2014. Ablation of PRDM16 and beige adipose causes metabolic dysfunction and a subcutaneous to visceral fat switch. Cell 156:304–316.

[32] Salans, L.B., Cushman, S.W., Weismann, R.E., 1973. Studies of Human Adipose Tissue adipose cell size and number in nonobese and obese patients. Journal of Clinical Investigation 52(4):929–941.

[33] Garaulet, M., Hernandez-Morante, J.J., Lujan, J., Tebar, F.J., Zamora, S., 2006. Relationship between fat cell size and number and fatty acid composition in adipose tissue from different fat depots in overweight/obese humans. International Journal of Obesity 30(6):899–905.

[34] Fabbrini, E., Sullivan, S., Klein, S., 2010. Obesity and nonalcoholic fatty liver disease: biochemical, metabolic and clinical implications. Hepatology 51(2): 679–689.

[35] Ouellet, V., Labbé, S.M., Blondin, D.P., Phoenix, S., Guérin, B., Haman, F., et al., 2012. Brown adipose tissue oxidative metabolism contributes to energy expenditure during acute cold exposure in humans. Journal of Clinical Investigation 122(2):545–552.

[36] Hoeke, G., Kooijman, S., Boon, M.R., Rensen, P.C.N., Berbeé, J.F.P., 2016. Role of brown fat in lipoprotein metabolism and atherosclerosis. Circulation Research 118(1):173–182.

[37] Dallner, O.S., Chernogubova, E., Brolinson, K.A., Bengtsson, T., 2006. β3-adrenergic receptors stimulate glucose uptake in brown adipocytes by two mechanisms independently of glucose transporter 4 translocation. Endocrinology 147(12):5730–5739.

[38] Hao, Q., Yadav, R., Basse, A.L., Petersen, S., Sonne, S.B., Rasmussen, S., et al., 2015. Transcriptome profiling of brown adipose tissue during cold exposure reveals extensive regulation of glucose metabolism. American Journal of Physiology - Endocrinology And Metabolism 308(5):E380–E392.

[39] Nelson, V.L., Jiang, Y.P., Dickman, K.G., Ballou, L.M., Lin, R.Z., 2014. Adipose tissue insulin resistance due to loss of PI3K p110α leads to decreased energy expenditure and obesity. American Journal of Physiology. Endocrinology and Metabolism 306(10):E1205–E1216.

[40] Solheim, M.H., Winnay, J.N., Batista, T.M., Molven, A., Njølstad, P.R., Kahn, C.R., 2018 May 3. Mice carrying a dominant-negative human PI 3-kinase mutation are protected from obesity and hepatic steatosis but not diabetes. Diabetes 67:1297–1309.

[41] Ueki, K., Fruman, D.A., Brachmann, S.M., Tseng, Y.H., Cantley, L.C., Kahn, C.R., 2002. Molecular balance between the regulatory and catalytic subunits of phosphoinositide 3-kinase regulates cell signaling and survival. Molecular and Cellular Biology 22:965–977.

[42] Ozcan, U., Cao, Q., Yilmaz, E., Lee, A.H., Iwakoshi, N.N., Ozdelen, E., et al., 2004. Endoplasmic reticulum stress links obesity, insulin action, and type 2 diabetes. Science 306(5695):457–461.

[43] Taniguchi, C.M., Aleman, J.O., Ueki, K., Luo, J., Asano, T., Kaneto, H., et al., 2007. The p85alpha regulatory subunit of phosphoinositide 3-kinase potentiates c-Jun N-terminal kinase-mediated insulin resistance. Molecular and Cellular Biology 27(8):2830–2840.

[44] Kosaki, A., Webster, N.J., 1993. Effect of dexamethasone on the alternative splicing of the insulin receptor mRNA and insulin action in HepG2 hepatoma cells. Journal of Biological Chemistry 268:21990–21996.

[45] Beneit, N., Fernández-García, C.E., Martín-Ventura, J.L., Perdomo, L., Escribano, Ó., Michel, J.B., et al., 2016. Expression of insulin receptor (IR) A and B isoforms, IGF-IR, and IR/IGF-IR hybrid receptors in vascular smooth muscle cells and their role in cell migration in atherosclerosis. Cardiovascular Diabetology 15(1):161.

[46] Beneit, N., Martín-Ventura, J.L., Rubio-Longás, C., Escribano, Ó., García-Gómez, G., Fernández, S., et al., 2018. Potential role of insulin receptor isoforms and IGF receptors in plaque instability of human and experimental atherosclerosis. Cardiovascular Diabetology 17(1):31.

[47] Blüher, M., 2016. Adipose tissue inflammation: a cause or consequence of obesity-related insulin resistance? Clinical Science 130(18):1603–1614.

[48] Gómez-Hernández, A., Beneit, N., Díaz-Castroverde, S., Escribano, Ó., 2016. Differential role of adipose tissues in obesity and related metabolic and vascular complications. The Internet Journal of Endocrinology 2016: 1216783.

[49] Cui, X.B., Chen, S.Y., 2017. White adipose tissue browning and obesity. The Journal of Biomedical Research 31(1):1–2.

[50] Bijland, S., Mancini, S.J., Salt, I.P., 2013. Role of AMP-activated protein kinase in adipose tissue metabolism and inflammation. Clinical Science 124(8):491–507.

[51] Yang, Q., Liang, X., Sun, X., Zhang, L., Fu, X., Rogers, C.J., et al., 2016. AMPK/α-Ketoglutarate Axis dynamically mediates DNA demethylation in the Prdm16 promoter and Brown adipogenesis. Cell Metabolism 24(4): 542–554.

[52] Wang, S., Liang, X., Yang, Q., Fu, X., Zhu, M., Rodgers, B.D., et al., 2017 Apr. Resveratrol enhances brown adipocyte formation and function by activating AMP-activated protein kinase (AMPK) α1 in mice fed high fat diet. Molecular Nutrition & Food Research 61(4). https://doi.org/10.1002/mnfr.201600746.

[53] Wang, S., Liang, X., Yang, Q., Fu, X., Rogers, C.J., Zhu, M., et al., 2015. Resveratrol induces brown-like adipocyte formation in white fat through activation of AMP-activated protein kinase (AMPK) α1. International Journal of Obesity 39(6):967–976.

[54] Zhang, F., Ai, W., Hu, X., Meng, Y., Yuan, C., Su, H., et al., 2018. Phytol stimulates the browning of white adipocytes through the activation of AMP-activated protein kinase (AMPK) α in mice fed high-fat diet. Food & function 9(4):2043–2050.

